Multi-rotor with Suspended Load: System Dynamics and Control Toolbox

Jan Erik Trachte, Luis Felipe Gonzalez Toro, Aaron McFadyen

1. Institute of Flight Mechanics University of Stuttgart 70569 Stuttgart, Germany
lrt67645@stud.uni-stuttgart.de
2. Science and Engineering Faculty, Queensland University of Technology, Australian Research Centre for Aerospace Automation (ARCAA) 4001 Brisbane, Australia
4008 Brisbane, Australia . felipe.gonzalez@qut.edu.au, aaron.mcfadyen@qut.edu.au

Abstract—**There is an increasing demand for Unmanned Aerial Systems (UAS) to carry suspended loads as this can provide significant benefits to several applications in agriculture, law enforcement and construction. The load impact on the underlying system dynamics should not be neglected as significant feedback forces may be induced on the vehicle during certain flight manoeuvres. The constant variation in operating point induced by the slung load also causes conventional controllers to demand increased control effort. Much research has focused on standard multi-rotor position and attitude control with and without a slung load. However, predictive control schemes, such as Nonlinear Model Predictive Control (NMPC), have not yet been fully explored. To this end, we present a novel controller for safe and precise operation of multi-rotors with heavy slung load in three dimensions. The paper describes a System Dynamics and Control Simulation Toolbox for use with MATLAB/SIMULINK which includes a detailed simulation of the multi-rotor and slung load as well as a predictive controller to manage the nonlinear dynamics whilst accounting for system constraints. It is demonstrated that the controller simultaneously tracks specified waypoints and actively damps large slung load oscillations. A linear-quadratic regulator (LQR) is derived and control performance is compared. Results show the improved performance of the predictive controller for a larger flight envelope, including aggressive manoeuvres and large slung load displacements. The computational cost remains relatively small, amenable to practical implementations.**

1. INTRODUCTION

Civilian application of Unmanned Aerial Systems (UAS) is spreading rapidly, including sectors such as construction, law enforcement, firefighting or agriculture . Small multirotor vehicles provide useful tools for automated farming by supporting plant biosecurity through surveillance like visual pest detection with the help of multi-spectral photography [1,2,3]. Whereas this is an established key feature of UAS, the actual treatment of affected areas often involves conventional methods, such as wide area pest spraying. However, autonomous multi-rotor aircraft could apply pesticides at high concentration and close proximity for less wind induced dispersal. External loads, suspended on a cable, may allow to spray a fluid right above or even inside a crop's canopy. Heavy suspended loads, no matter if containing a sensor, water for fire fighting or a pesticide fluid, may significantly influence flight dynamics due to a high mass-ratio of the load to the vehicle. To this end, control of lightweight aerial vehicles should not neglect consideration of the external load to ensure safe and precise flight trajectories. The nonlinear dynamics of an aerial suspended load are well studied by a vast amount of publications, such as [5–8]. In most cases, the controller is derived by a linearisation of the dynamical model. [5] provides an overview of the generic 3-dimensional pendulum control problem. [6] introduces a fuzzy controller for load swing compensation while the vehicle is tracking a position trajectory at low attitude angles near hover. Detailed studies on the slung load model and a trajectory tracking slung load controller using linear quadratic regulation are presented in [7]. [8] investigates particularly the control of a quadrotor with a slung load. A dynamic programming approach is developed, capable to generate swing free trajectories for agile manoeuvres.

Nevertheless, there hasn't been research on including the slung load dynamics to the model of an online Nonlinear Model Predictive Control (NMPC). NMPC provides an optimal controller for highly nonlinear dynamics whilst accounting for constraints and enabling a state feedback loop that involves disturbance and model uncertainties. NMPC is an established tool for relatively slow elapsing processes since the Nineties and has mostly been applied in the field of industrial process engineering. However, due to rising computational power on micro controllers, NMPC becomes applicable for agile lightweight aerial systems, too.

To this end, the contributions of this paper are:

1. Design of a NMPC for a quadrotor with suspended slung load, capable of stabilising or tracking the load and quad movement over a large flight envelope
2. Performance comparison of the NMPC to a Linear Quadratic Regulator (LQR) with respect to robustness, time varying reference and aggressive control
3. Preparation of a NMPC algorithm in C++ code for field tests including assessment of computational demand

This paper is structured as follows: Section 2 outlines the complete derivation of the nonlinear model. The NMPC control design and associated simulation framework are presented in section 3 and 4 respectively. Simulation results are summarised in section 5 followed by a discussion in section 6 and conclusion/outlook in section 7.

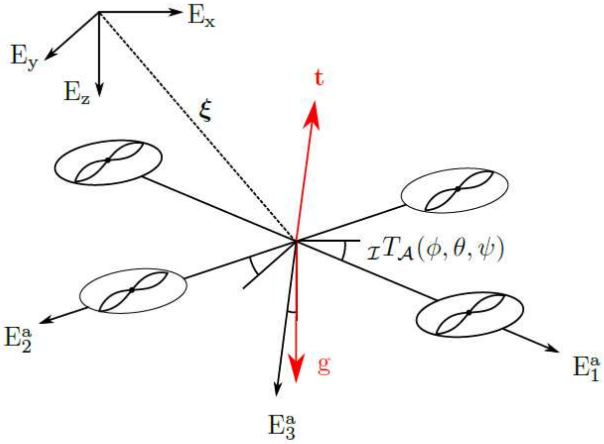

Figure 1. Point mass model of the quadrotor with body frame A and inertial frame I.

2. SYSTEM DYNAMICS

A precise derivation of the highly non-linear system dynamics of the quad-load-combination is essential for an efficient control over the entire flight envelope. This section sequentially describes the derivation of the dynamic equations for the quadrotor and suspended slung load subject to the quad control inputs.

Quadrotor dynamics

The model of the quad kinematics is based on the assumption that the vehicle can be considered as a single point mass with a tilting thrust vector tI and a constant gravity vector g in the inertial frame. This simplification is known to be adequate for control design as the attitude controller is assumed to be much faster than the position controller [9, 10]. The inertial frame I= $\{E_x,E_y,E_z\}$ is defined. The position of the body frame's origin in I is $\xi=(x,y,z)$. The matrix I_TA, also called directional cosine matrix, describes the rotation of A to I, hence containing the Euler angles of the quad frame. The quadrotor acceleration in I reads

$$\begin{pmatrix}\ddot{x}\\ \ddot{y}\\ \ddot{z}\end{pmatrix}_{\mathcal{I}} = \underbrace{{}_{\mathcal{I}}T_{\mathcal{A}}\begin{pmatrix}0\\ 0\\ T/\mathrm{M}\end{pmatrix}_{\mathcal{A}}}_{\mathbf{t}_{\mathcal{I}}} + \begin{pmatrix}0\\ 0\\ \mathrm{g}\end{pmatrix}_{\mathcal{I}},$$

where T is the collective thrust scalar, that is considered to be only directed into an upwards direction of the body frame A. M is the mass of the vehicle and g is the gravitational constant pointing downwards in I. The directional cosine matrix contains cardanian rotations of the three euler angles yaw, pitch and roll (ψ, θ, ϕ). The transformation reads $_{\mathcal{I}}T_{\mathcal{A}} = T_3(\psi)T_2(\theta)T_1(\phi)$ and after performing the matrix multiplications becomes

$$_{\mathcal{I}}T_{\mathcal{A}} = \begin{pmatrix} c\psi c\theta & c\psi s\phi s\theta - c\phi s\psi & s\phi s\psi + c\phi c\psi s\theta \\ c\theta s\psi & c\phi c\psi + s\phi s\psi s\theta & c\phi s\psi s\theta - c\psi s\phi \\ -s\theta & c\theta s\phi & c\phi c\theta \end{pmatrix}$$

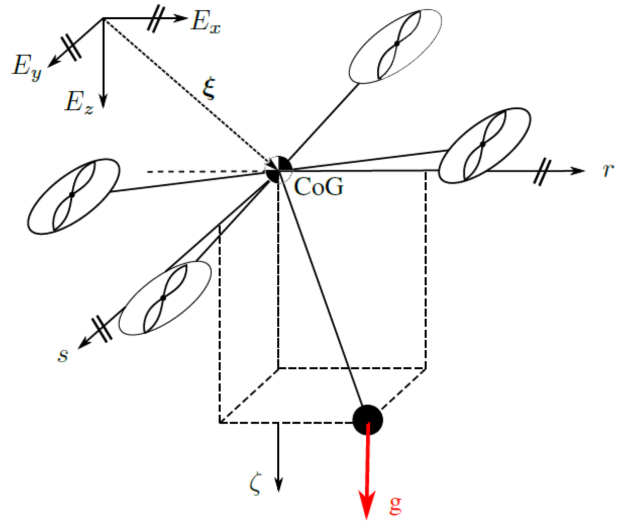

Figure 2. Load coordinates in frame O related to inertial frame I by the quad position ς.

Suspended Slung Load

Several assumptions are made for the kinematics of the cable suspended slung load. These are:

- No aerodynamic effects
- No cable mass
- No cable strain
- No free fall of the load (cable force ≥ 0)
- Pivot has no offset to the quad's Centre of Gravity (CoG)
- Heavy load, i.e. non-negligible influence to flight dynamics

This allows the reduction of the equations of motion to the movement of the load on a sphere's surface similar to [7].
We first introduce the load frame O with its orientation corresponding to the inertial frame I as shown in Fig. 2. The origin of O is in the quad's CoG, where the load positions r; s; ς are parallel to E_x,E_y,E_z respectively.

The constraint of the load being on the surface of a sphere with the cable length l leads to

$$\zeta = \sqrt{\mathrm{l}^2 - r^2 - s^2}$$

for $\varsigma_L \geq 0$. The latter is an acceptable restriction, because the structural design does not allow the load to swing to the upper hemisphere above the quad. Yet we have to keep in mind that an up-swinging of the load must be avoided and could violate the optimal control problem of the predictive controller. The dynamic model would produce complex state vector numbers, leading to a non-global solution that does not allow an application of appropriate control inputs. To this end, additional constraints for the optimal control problem have to be made.

The Lagrangian function, representing the kinetic and potential energy of the load, reads

$$\mathscr{L} = \frac{1}{2}\left((\dot{x}+\dot{r})^2 + (\dot{y}+\dot{s})^2 + (\dot{z}+\dot{\zeta})^2\right) - \mathrm{g}(z+\zeta)$$

and the Euler-Lagrange equations are

$$\frac{\mathrm{d}}{\mathrm{dt}}\left(\frac{\partial\mathscr{L}}{\partial\dot{r}}\right) = \frac{\partial\mathscr{L}}{\partial r}$$
$$\frac{\mathrm{d}}{\mathrm{dt}}\left(\frac{\partial\mathscr{L}}{\partial\dot{s}}\right) = \frac{\partial\mathscr{L}}{\partial s}$$

We insert equation 4 and 5 into 6 and solve for the load acceleration $\ddot{r}, \ddot{s}$. We then retrieve the equations of motion of the slung load subject to the quad's acceleration. The equation in its entirety can be found in [10].

Deriving the cable force

As we assume the suspended load to have a non-negligible influence on the quadrotor flight dynamics, the resulting cable force is derived in this section and then included to the entire combined model. According to Newton's second law of motion, the cable force is derived by multiplying its absolute acceleration with its mass. The gravitational impact has to be added separately and depends on the load's deflection. The equation for the cable force then is

$$\mathbf{f} = -\mathrm{m}\begin{pmatrix} \ddot{x}+\ddot{r} \\ \ddot{y}+\ddot{s} \\ \ddot{z}+\ddot{\zeta}-\mathrm{g}\,(\zeta/\mathrm{l}) \end{pmatrix}$$

where m is the load mass, g is the gravitational constant and l the length of the cable.

Coupled Dynamics

The kinematics of the load depend on the moving pivot and herewith the quad acceleration. The acceleration resulting from the cable force impact on the pivot is now added to the quad acceleration. With Newton's second law of motion, this is ac = f/M, where f is the cable force vector and M is the quad mass. The complete system of equations for the combined dynamics is shown in (8). It remains to mention that, as a result, the quad dynamics implicitly depend on the load's motion and vice versa. The yaw angle   is considered to be constant zero such that a feed forward term can be added to control the quadrotor orientation.

3. CONTROL DESIGN

The control design is separated into the description of the NMPC and the LQR, both of which are used and compared in this work. The two controls consider the slung load dynamics to derive the corresponding controller.

Nonlinear Model Predictive Control (NMPC)

The mathematical model defined by (8) represents the system dynamics and is used as an internal model f for the predictive controller. An optimal control problem is repeatedly solved at each control step over a finite time horizon [8]. The state vector $x = (x, y, z, u, v, w, \psi, \theta, \phi, \dot{r}, \dot{s})$

Table 1. Inequality constraints for NMPC

Description	Constraint
Roll angle limit	$\pi/2 \leq \phi \leq \pi/2$
Pitch angle limit	$\pi/2 \leq \theta \leq \pi/2$
Sph. surface constr. (r)	$-1 \leq r/\sqrt{\mathrm{l}^2 - s^2} \leq 1$
Sph. surface constr. (s)	$-1 \leq s/\sqrt{\mathrm{l}^2 - r^2} \leq 1$
Roll rate limit	$-\pi \leq \dot{\phi} \leq \pi$
Pitch rate limit	$-\pi \leq \dot{\theta} \leq \pi$
Collective thrust range	$-1.6\mathrm{Mg} \leq T \leq -0.4\mathrm{Mg}$

It contains the three Cartesian positions and velocity of the vehicle, the pitch and roll angle as well as the two slung load Cartesian coordinates and their derivatives. The third coordinate is omitted due to the spherical surface constraint of (4). The control vector u = $\dot{\phi}, \dot{\theta}, T$ contains the vehicle's roll rate, pitch rate and collective thrust. A cost function J is minimized with respect to u. The cost function is used to penalise deviation from the reference flight and slung load condition. The optimal control problem can be defined as

$$J^\star(\mathbf{x},\mathbf{u}) = \underset{\mathbb{U}}{\operatorname{argmin}}\, J(\mathbf{x},\mathbf{u})$$

$$J(\mathbf{x},\mathbf{u}) = \Delta\mathbf{x}_N^T P \Delta\mathbf{x}_N + \sum_{k=1}^{N-1} \Delta\mathbf{x}_k^T Q \Delta\mathbf{x}_k + \Delta\mathbf{u}_k^T R \Delta\mathbf{u}_k\ ,$$

$$\begin{aligned} \text{where} \qquad & \Delta\mathbf{x}_k = \mathbf{x}_k - \mathbf{x}_k^* \\ & \Delta\mathbf{u}_k = \mathbf{u}_k - \mathbf{u}_k^* \\ \text{subject to} \qquad & \mathbf{x}_k \in \mathbb{X} \quad \mathbb{X} \in \mathbb{R}^{12} \\ & \mathbf{u}_k \in \mathbb{U} \quad \mathbb{U} \in \mathbb{R}^3 \\ & \mathbf{x}_{k+1} = f(\mathbf{x}_k, \mathbf{u}_k) \end{aligned}$$

with the errors Δx_k and Δu_k of the current state and control to the reference trajectory, denoted by the asterisk. The matrices Q and R are positive semi-definite weighting matrices on the quadratic state error and control error respectively. P defines the terminal cost, i.e. the positive cost of the error at the last step of the prediction horizon. The stability of the open loop can be significantly influenced by this parameter. The ACADO toolkit [12] provides a comprehensive C++ code library suitable for creation of an algorithm to solve the optimal control problems arising from the NMPC formulation.

The optimal control problem is subject to the model's differential system of equations and a set of inequality constraints. These constraints capture the bounds on the control inputs and platform limitations, or state constraints. For example, they can be used to prevent the platform from flying upside down (through roll and pitch angle bounds) or limit the roll rate based on the maximum torque that the rotors can generate. The collective thrust is limited to the maximum available power and to avoid an unrecoverable drop in altitude. The constraint domain is derived from experience or specification of the X-4 Flyer Mark II in [13], with numerical values given in Table 1.

$$\ddot{x} = \left(T\cos\phi\sin\theta - \mathrm{m}(\ddot{x}+\ddot{r})\right)/\mathrm{M}$$
$$\ddot{y} = -\left(T\sin\phi - \mathrm{m}(\ddot{u}+\ddot{s})\right)/\mathrm{M}$$
$$\ddot{z} = \left(T\cos\phi\cos\theta + \mathrm{m}((\ddot{r}r+\dot{r}^2+\ddot{s}s+\dot{s}^2)/\zeta - \ddot{z} + (\dot{r}r+\dot{s}s)^2/\zeta^3 + \mathrm{g}(\zeta/\mathrm{l}))\right)/\mathrm{M} + \mathrm{g}$$
$$\ddot{r} = (\zeta^4\ddot{x} - r\zeta^3\ddot{z} + rs\zeta^2\ddot{s} + (r\mathrm{l}^2 - rs^2)\dot{r}^2 + (r\mathrm{l}^2 - r^3)\dot{s}^2 + 2\dot{r}\dot{s}r^2s + r\mathrm{g}\zeta^3)/((s^2-\mathrm{l}^2)\zeta^2)$$
$$\ddot{s} = (\zeta^4\ddot{y} - s\zeta^3\ddot{z} + rs\zeta^2\ddot{r} + (s\mathrm{l}^2 - sr^2)\dot{s}^2 + (s\mathrm{l}^2 - s^3)\dot{r}^2 + 2\dot{r}\dot{s}s^2r + s\mathrm{g}\zeta^3)/((r^2-\mathrm{l}^2)\zeta^2)$$

Table 2. Overview of NMPC settings

Parameter	Value
Number of time-steps N	30
Time step size δ	0.4 s
Discretisation type	Multiple Shooting
Integrator type	Gauss-Legendre 3rd Order
Integrations per step N_i	4

The reference trajectories and weighting matrices are set dynamically in the simulation framework outlined in section 4. An overview of the prediction parameters and their numerical values are given in Table 2. Values were chosen empirically and based on literature, such as [14,15] or examples from the ACADO toolkit.

Linear Quadratic Regulator (LQR)

The same dynamic model, used for the NMPC controller, is used to derive the LQR. The nonlinear dynamic model (8) is linearised about hover such that $\dot{x} = Ax + Bu$. As the system\ is both, controllable and observable, an LQR controller can be derived by minimising a quadratic cost function similar to (10) over a inifinite horizon such that

$$\text{minimise} \quad J = \sum_{k=0}^{\infty} \mathrm{x}^{\mathrm{T}} Q \mathrm{x} + \mathrm{u}^{\mathrm{T}} R \mathrm{u}$$

A feedback control gain matrix K can then be derived from the solution of the associated Riccati equation [16, 17] that arises from solving (11). The control law is then *u = -Kx.*

4. SIMULATION FRAMEWORK

The simulation framework can be structured into six major components. These are:

- Top-level controller (i.e. NMPC or LQR)
- Low-level proportional attitude control
- Control mixer to provide motor-speeds
- Quadrotor system dynamics
  Slung load system dynamics
- Visualisation tool

Fig. 3 gives an overview on the correlation of the components and the following paragraphs give a detailed explanation on each, starting from the top-level controller.

The top-level control is embedded to the framework by an outer feedback loop, where the states are directly forwarded to the control block, neglecting measurement deviations, hence *y = x*. Whilst the LQR is included by putting the gain matrix K on the state error, the NMPC uses a MATLAB S function and C++ compiler (mex) to define the controller. Reference trajectories and weighting matrices are dynamically allocated in the SIMULINK environment.

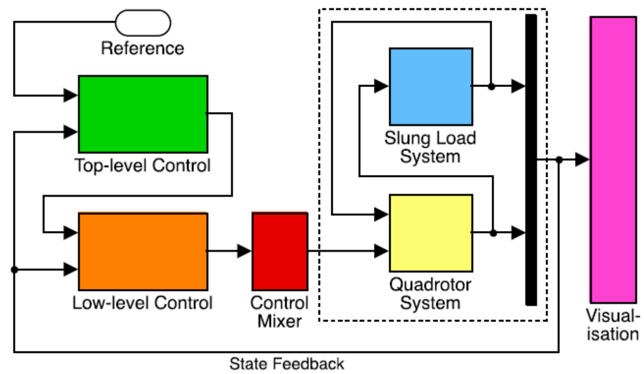

Figure 3. Correlation of major simulation framework components.

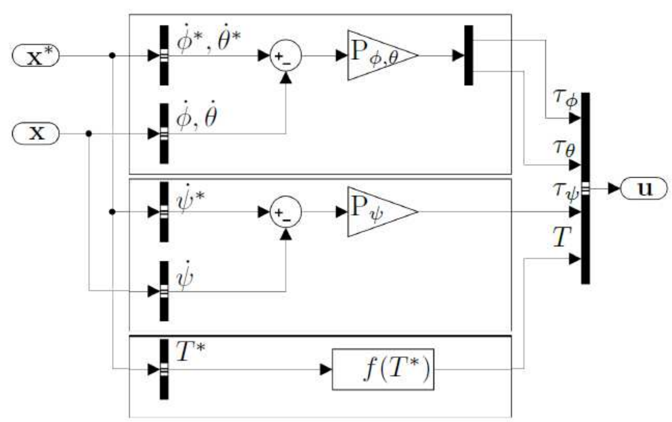

Figure 4. Low-level proportion control design.

The NMPC or LQR controller provide the desired roll/pitch rate and the collective thrust. However, the simulation framework requires desired Euler angle deflections at this point. To this end, we introduce a low-level proportion state feedback control. Fig. 4 shows the flow chart of this controller. The parameters of the gains on the error feedback are chosen on the basis of a simulation by [18]. The desired motor-speeds for the collective thrust are derived using [13] by using the relationship between the absolute thrust to the motor speed, rotor area, air density and thrust coefficient.

The output of the low-level control needs to be mixed in order to provide the individual motor speeds that correspond to the desired Euler angle deflection.

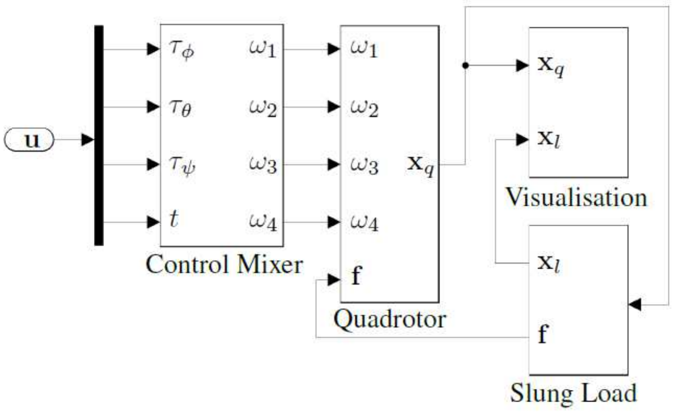

Figure 5. Flow chart of the simulation framework excluding the regulators.

Table 3. Overview on physical simulation parameters

Parameter	Symbol	Value
Gravity constant	g	$9.81\,\mathrm{m\,s^{-2}}$
Vehicle mass	M	$4.0\,\mathrm{kg}$
Load mass	m	$1.5\,\mathrm{kg}$
Cable length	l	$1.5\,\mathrm{m}$
Rotor coefficient	b	$1.32 \times 10^{-5}\,\mathrm{N\,s^2}$
Max. motor-speed	$\omega_{\max}$	$1090\,\mathrm{s^{-1}}$

Fig. 5 shows the detailed correlation of the mixer, the quad and load system and the visualisation module. The mixer translates the required angle deflections Ti and collective thrust T into valid, limited motor-speed values wi. This is done by distributing the input to the corresponding rotor. The control mixer does not include any state feedback control and directly forwards the required motor-speeds to the quadrotor model.

The quadrotor system is based on the SIMULINK model of the X-4 Flyer Mark II by [13], and available in [18]. The model represents accurate flight dynamics including aerodynamic effects, such as blade flapping and pitch/roll damping.

The model is not the same as the one used in the NMPC or LQR and is considered to be more realistic.

The slung load system (7) is separate to the quadrotor component and connected as shown in Fig. 5. The quad state is forwarded to the slung load module to derive the loads movement due to the quad's acceleration. The cable force, induced by the gravitational impact and kinematics on the load, is then forwarded to the quadrotor system which influences the flight dynamics. Table 3 gives an overview of the physical parameters of the dynamic systems. The maximum motor-speed of the X-4 Flyer Mark II was changed from 1000 rad s^{-1} to 1090 rad s^{-1} to enable a 60% control margin, allowing the vehicle to manoeuvre with heavy slung loads up to 2 kg. The original specification of the X-4 allows the carriage of 1 kg fixed loads.

The state of the quad and slung load are forwarded to plotting module for a visualisation of the vehicle and the slung load. Time dependant plots of particular states, as well as a real time 3-dimensional simulation, based on [18] are included.

Table 4. Weighting matrix variations

Matrix Cell	Value	Corresp. state/control
$Q(3,3)$	1×10^3	quad position z
$Q(7,7)$	1×10^2	load position r
$Q(8,8)$	1×10^2	load position s

Several limitations on the simulation framework must be kept in mind. Natural appearance of system disturbance and observer/sensor noise is neglected. Also the slung load model will deflect to realistic behaviour, due to the limitations made in section 2. The control of the yaw angle is neglected in this work, but is included in the vehicle dynamics of the simulation. To keep realistic results, without inserting yaw dynamics to the top-level controllers, a minimalistic proportional control is used to explicitly keep the yaw angle at zero. The control effort for this achievement is small and will be neglected since the yaw rotation is not subject to any direct disturbance in the simulation. The proportional gain value of the yaw control is again based on a simulation by [18].

5. RESULTS

The NMPC and the LQR are evaluated for their capability of managing stabilisation problems and trajectory tracking. Four different scenarios are analysed. The first two scenarios involve stabilisation problems with a deflected initial condition and a non-predictable external disturbance. The second two scenarios involve reference trajectory tracking for the quadrotor and the load position.

The weighting matrices of both control algorithms are the same in each simulation. Table 4 shows the entries of the matrices that show variations to the identity matrix. The weighting matrix P for the NMPC terminal state error is set equal to the corresponding values of Q for simplification.

Stabilisation of Load Displacement

In this scenario the goal is to actively damp an oscillation of the load. The quad is at stable hover and the load is initially displaced from its equilibrium position by 1m to the positive r-direction. As the control reference is set to maintain a stable hover with no load movement, active damping of the swinging load is required. Fig. 6 compares the vehicle's x- position, the load's position r and the corresponding control input $\dot{\theta}$, i.e. pitch-rate, for the NMPC and the LQR control designs. The

LQR forces the control limits to be exceeded and a motor-speed beyond the possible limit is demanded on some rotors. As a result, the load contacts the ground and the yaw angle deviates from the reference value. Both can be compensated after a few seconds, when the pitch angle and corresponding thrust demand start decreasing. The NMPC ensures the control constraints are respected, such that the load no longer impacts the ground. Of note, both controllers are able to damp the load within 4 s, whilst returning the platform to the reference flight configuration.

Stabilisation of Wind Disturbance

In this scenario the goal is to compensate an external disturbance that is not included in the prediction model. A variable wind speed v_w is implemented to the simulation framework. The wind speed implements the mathematical representation for a wind gust according to the Military Specification [19].

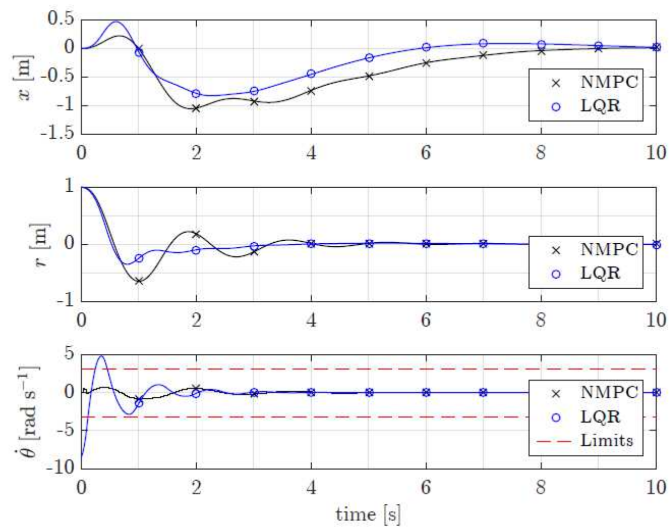

Figure 6. Plot of the quad position, load position and commanded pitch rate over time with an initial load deflection.

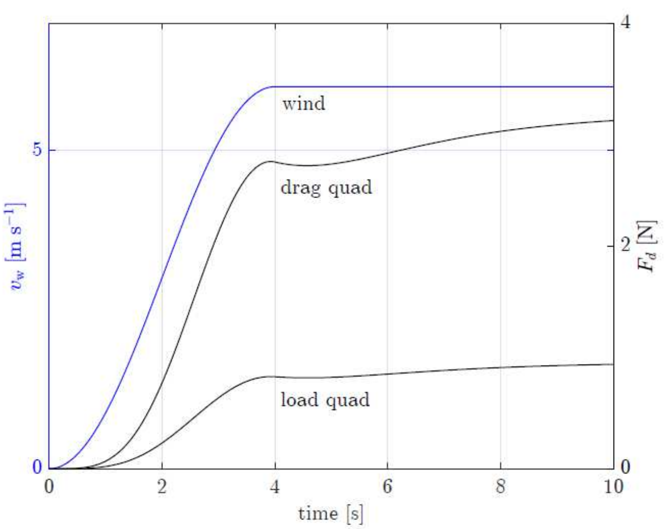

Figure 7. Wind speed profile and resulting drag force.

The difference of the wind-speed to speed of the body frame A is converted into a drag force that is impacting both, the vehicle and the load. The drag force is derived by input $Fd = 0.5\rho v_w{}^2 CdA$ where the drag coefficient Cd and the vehicle/load reference area A are estimated. The air density ρ is adopted from [13]. Fig. 7 shows the wind speed in x-direction by the solid blue line and the left scale. The right scale and the black lines represent the resulting drag forces, that also depend on the body movement induced by the NMPC control response. The additional velocity of the load's movement inside the body frame A is neglected. The performance of the NMPC and the LQR control design in this simulation scenario is shown in Fig. 8 through the quad position x, the load position r and the relevant control input $\dot{\theta}$. The reference is the initial position of quadrotor and load.

Waypoint Tracking

In this scenario, the goal is to track a specific reference rajectory for the platform whilst avoiding a swinging of the load.

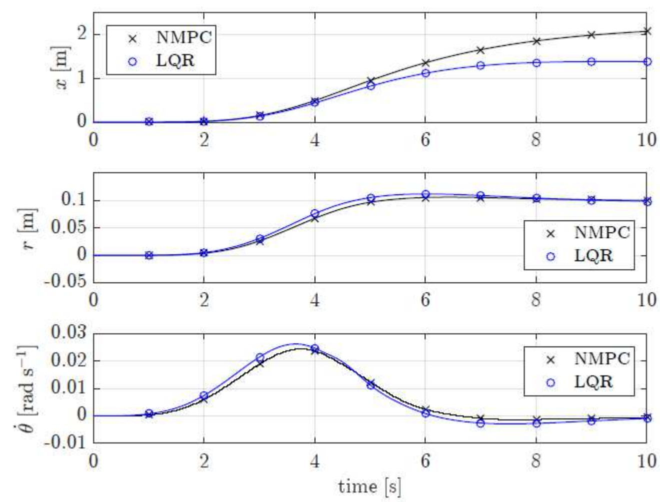

Figure 8. Quad position x, load position r and control input $\dot{\theta}$ under influence of a wind gust in positive x-direction.

An inclined square circuit is used as the reference trajectory for the vehicle, where each corner forms a waypoint at a different reference altitude. The square's sides are 1m in length (only lateral direction measured) with an altitude variation of ±2 m. The load reference is zero deflection to the equilibrium state, i.e. no swinging. The initial position is at stable hover with non-deflected slung load and an altitude of 2 m. Results for an example simulation are depicted in Fig. 9, where quad and load position are shown.

The results suggest that the NMPC is able to effectively track the reference trajectory of both the quad and the load, with a Root Mean Squared Displacement (RMSD) of 0.064m and 0.091m respectively. The LQR control design shows poorer tracking performance, approximating a more circular trajectory with position and load RMSD of 0.569m (governed by the altitude deviation) and 0.021m respectively. This can be attributed, in part, to the fact a single reference value is required at each time step for the LQR, compared to the full time varying reference used in the NMPC. The result implies that the NMPC approach can better manage more complex reference trajectories.

Load Position Tracking

In this scenario, the goal is to track a specific load reference trajectory, whilst the platform maintains hover. The load reference describes a circular pattern of radius 1m and a period of 3 s, such that

$$r^{*} = \cos\left(\frac{2\pi}{3}t\right) \text{ and } s^{*} = \sin\left(\frac{2\pi}{3}t\right)$$

The initial position of the platform and load are (0, 0,-2) and (0, 0,-2+l) respectively. Results for an example simulation are given in Fig. 10, where load and platform position are depicted.

To track the reference load position, the quad must first leave the stable hover in order to move or upswing the load. The flight path for both control algorithms describes loops, where a larger loop radius is initially required to force the load to adopt the reference trajectory. Subsequent motion is a relatively constant radius circular trajectory to maintain the load's reference circular path. The NMPC's performs with an overall RMSD of quad and load position of 0:779m and 0:915m respectively. The LQR comes to 0:781m and 0:924 m.

The load trajectory generated by the LQR touches the ground at 0:8 s simulation time, shown by the dashed line. The actual ground contact is not part of the simulation and the depicted flight neglects the impact to continue the flight and recover from the altitude drop at 2:2 s simulation time. The reason for this impact is again the disregarding of control input constraints, putting the vehicle to an attitude where total thrust becomes insufficient for maintaining a level flight. Remark The average computational cost of the NMPC is 5:0 ms per real time iteration which corresponds to 200 Hz control sample time. This was verified using 1000+ iterations on the first stabilisation scenario run on a 1.7 GHz Intel Core i7-4650U dual-core processor on an Apple OS X 10.9.5 operating system and a test-simulation in C++ code. The SIMULINK environment was removed to ensure efficiency of the control algorithm. Similar computation times were observed for other scenarios which suggest the controller is suitable for real applications, and could be implemented onboard real hardware configurations.

6. DISCUSSION

The LQR generally shows immediate control response when deflected from the reference state. This can be seen in the first scenario, where the load is initially deflected and shall be damped by the control. The LQR instantly responds with a high pitch-rate command to counter the swinging load, without consideration of any constraints. Not only the pitch-rate itself, but also the tilted thrust vector both demand additional thrust, i.e. motor-speed of the rotors. The system is not capable of providing the required thrust, leading to a loss in altitude and yaw control failure. The NMPC shows better accuracy in z-direction generally, although the same penalty value is set on the state error of z. It is assumed that the linear dynamics of the LQR cannot adequately approximate the system dynamics at high attitude angles (pitch and roll), and in particular, the required increase in thrust. The NMPC significantly reduces control effort by accounting future control commands and considering constraints unlike the LQR.

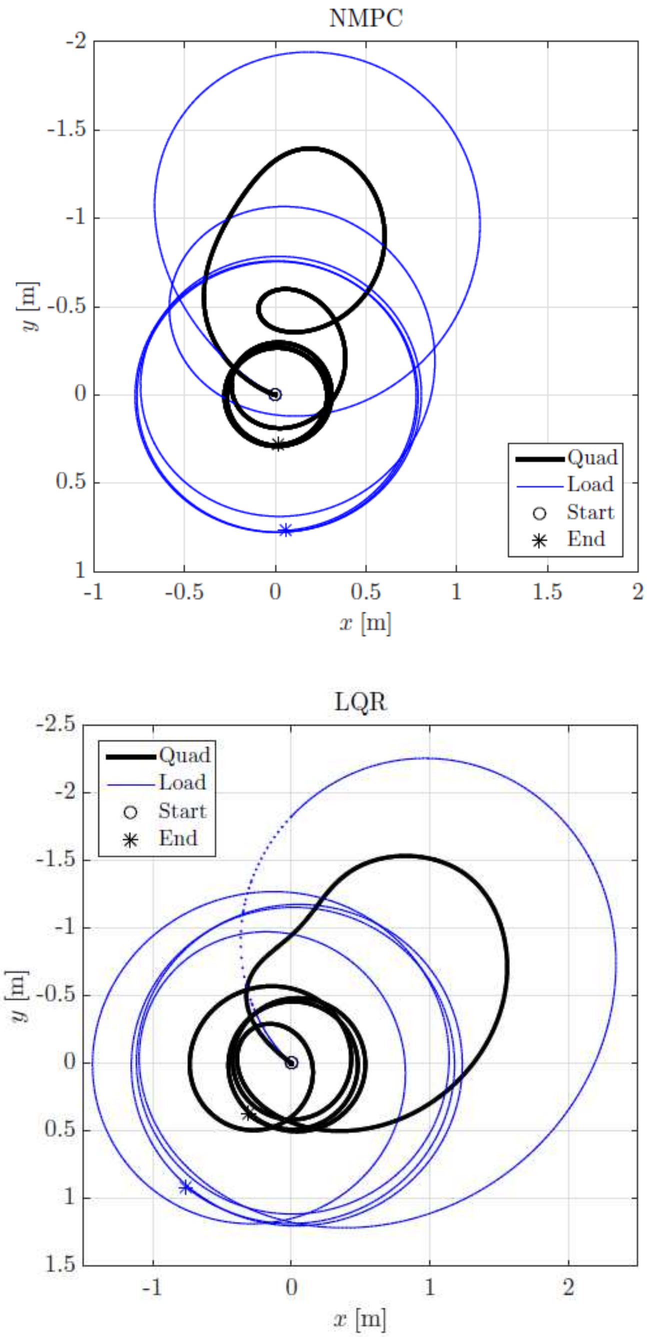

Figure 10. Tracking a circular load reference of radius 1m to the quad and period 3 s while quad reference is at origin.

Based on the design, both control algorithms are unable to maintain the reference position under a persistent disturbance such as wind and model mismatch. The NMPC gives more consideration to the slung load position, although a constant load deflection cannot be avoided, due to the fixed definition of the disturbance. Load deflection and control effort of the NMPC is slightly smaller than the LQR, yet both algorithms show poor and similar performance.

Capability of considering the future impact of each control action also facilitates precise and efficient tracking of a reference trajectory. The LQR however shows significant deviation from the reference trajectory of the quad, due to the lack of accounting conditions for a turn before the waypoint is actually reached. The predictive nature of the NMPC becomes apparent when comparing the third and the last waypoint corner of the square in the first trajectory tracking scenario. The NMPC takes a shortcut on the third corner to smoothly continue the flight to the last waypoint, whereas the last point is reached precisely with a full stop. The initial excitation of the load to reach the circular path occurs smooth and with consideration of the control effort and constraints. The LQR's initial control command results in a ground contact of the load.

Nevertheless, the LQR is basically able to manoeuvre the quad onto the stable circular trajectory, just as the NMPC, even though requiring more deviation to the quad position reference.

Computational expense of the NMPC is significantly higher than the LQR or other conventional control algorithms. However, it is shown that the derived code is capable to perform control steps at a sample rate close to 200 Hz, eligible for low-level control of a multi-rotor system.

7. CONCLUSION

A NMPC algorithm for slung load quadrotor control including comparative performance assessment under a range of operating conditions was presented. The results show the importance of explicit consideration of the platform constraints and nonlinear dynamics of slung load systems in control design. Especially when heavy slung loads generate significant cable forces, wise trajectory planning is required. This work shows that the LQR may violate these constraints, .g. leading to ground contact. The NMPC strictly avoids such events and significantly decreases the overall control effort through predictive management of the actuating control elements. This is a great advantage when power is limited, e.g. carrying loads close to the specification limit, resulting in short control margins. Both optimal control algorithms show poor performance, when non-predictable disturbance or model uncertainties occur.

Possible methods for counterfeiting these issues could be the addition of an integral action or a learning based model predictive control, as investigated in [13].

Further research on the presented application of NMPC should include implementation to real flight. A state observer for the slung load must be derived, which could be accomplished using visual sensor to then realise an integrated visual predictive control solution [20]. Investigation on the NMPC robustness, e.g. Lyapunov stability using the end term penalty, is advisable to assure robustness for all operating conditions before preparing a field deployable solution. The use of FPGA for autonomous unmanned aerial vehicle [21] on-board MPC is also under investigation

ACKNOWLEDGMENTS

This work was kindly supported by Queensland University of Technology (QUT), Australian Research Centre for Aerospace Automation (ARCAA) and Plant Biosecurity CRC. The authors would also like to thank Walter Fichter and Christoph Seiferth at the Institute of Flight Mechanics and Control (IFR), University of Stuttgart in Germany.

REFERENCES

[1] C. Hillnh¨utter et al., "Remote sensing for the detection of soil-borne plant parasitic nematodes and fungal pathogens," in Precision Crop Protection-the Challenge and Use of Heterogeneity, Springer, 2010, pp. 151–165.

[2] F.Gonzalez, MPG Castro, P. Narayan, R. Walker. L. Zeller "Development of an autonomous unmanned aerial system to collect time□stamped samples from the atmosphere and localize potential pathogen sources" Journal of Field Robotics 28 (6), 961-976, 2009.

[3] D.S. Lee, L.F. Gonzalez, K. Srinivas, D.J. Auld, J. Periaux. "Multi-objective/multidisciplinary design optimisation of blended wing body UAV via advanced evolutionary algorithms" Collection of technical papers. 45th AIAA aerospace sciences meeting 1, 296-316

[4] L.F .Gonzalez, DS Lee, R.A Walker, J. Periaux " Optimal mission path planning (MPP) for an air sampling unmanned aerial system "Proceedings of the Austral-Asian Conference on Robotics and Automation, 2009

[5] J. Shen et al., "Dynamics and control of a 3d pendulum," in Conference on Decision and Control, The Bahamas, 2004, pp. 323–328.

[6] H. M. Omar, "New fuzzy-based anti-swing controller for helicopter slung-load system near hover," in Int. Symp. Computational Intelligence in Robotics and Automation, Daejeon, Korea, 2009, pp. 474–479.

[7] M. Bisgaard, "Modeling, estimation, and control of helicopter slung load system," Ph.D. dissertation, Fac. Eng. and Science, Aalborg Univ. Space Center, 2007, pp. 204–221.

[8] I. Palunko et al., "Trajectory generation for swingfree maneuvers of a quadrotor with suspended payload: A dynamic programming approach," in Int. Conf. on Robotics and Automation, St. Paul, MN, 2012, pp. 2691–2697.

[9] M. Burri et al., "Aerial service robots for visual inspection of thermal power plant boiler systems," in Int. Conf. on Applied Robotics for the Power Industry, Zurich, Switzerland, 2012, pp. 70–75.

[10] M. Hehn and R. D'Andrea, "A flying inverted pendulum," in Int. Conf. on Robotics and Automation, Shanghai, China, 2011, pp. 763–770.

[11] R. Findeisen, and F. Allg¨ower, "An introduction to nonlinear model predictive control," in Benelux Meeting on Systems and Control, Veldhoven, The Netherlands, 2002, pp. 119-141.

[12] B. Houska et al., "ACADO toolkit—An open-source framework for automatic control and dynamic optimization," Optimal Control Applications and Methods, vol. 32, no. 3, pp. 298–312, 2011.

[13] [P. Pounds et al., "Modelling and control of a large quadrotor robot," IFAC Control Engineering Practice, vol. 18, no. 7, pp. 691–699, 2010.

[14] P. Bouffard, “On-board Model Predictive Control of a Quadrotor Helicopter: Design, Implementation, and Experiments,” Univ. of California, Berkeley, CA, 2012.
[15] K. Alexis et al., “Model predictive quadrotor control: attitude, altitude and position experimental studies,” IET Control Theory and Applications, vol. 6, no. 12, pp. 1812–1827, 2012.
[16] Matlab User’s Guide, The Math Works Inc., 2013.
[17] D. E. Kirk, Optimal control theory: an introduction, Courier Dover Publications, 2012.
[18] P. Corke, “A robotics toolbox for MATLAB,” IEEE Robotics and Automation Magazine, vol. 3, no. 1, pp. 24–32, 1996.
[19] D. Moorhouse, and R.Woodcock, “US Military Specification MILF8785C,” US Department of Defense, 1980.
[20] A. Mcfadyen et al., “Aircraft collision avoidance using spherical visual predictive control and single point features,” in Int. Conf. on Intelligent Robots and Systems, Tokyo, Japan, 2013, pp. 50–56.
[21] J. Kok, L.F. Gonzalez, N. Kelson " FPGA implementation of an evolutionary algorithm for autonomous unmanned aerial vehicle on-board path planning" Evolutionary Computation, IEEE Transactions on 17 (2), 272-281, 2013

BIOGRAPHY

Jan Erik Trachte is a current candidate for the degree of an aerospace engineering diploma at the University of Stuttgart, Germany. His majors are in fluid dynamics as well as flight mechanics and control, for which he studied optimal control on rotary aircraft at Queensland University of Technology (QUT) in Brisbane, Australia for nine months as part of the here presented work. His interests combine theoretical fundamental research and early application/prototyping. He was a research assistant at the e-Genius project, an electric experimental motorglider and holds a Private Pilot License for single-engine aircraft and gliders.

Luis Felipe Gonzalez Toro is a Senior Lecturer (UAV) in the Science and Engineering Faculty, QUT. He holds a BEng (Mech) and a PhD from the University of Sydney. His research explores bioinspired optimisation, uncertainty based UAV path planning and UAVs for environmental monitoring and plant biosecurity. He leads the CRC Plant Biosecurity project Evaluating Unmanned Aerial Systems for Deployment in Plant Biosecurity and the Green Falcon Solar Powered UAV. Felipe is a Chartered Professional Engineer and member of professional organisations including the RAeS, IEEE and AIAA. He is also an EDN, iENA Innovation award winner and holds a Private Pilot Licence.

Aaron McFadyen is a Research Engineer and PhD student at the Australian Research Centre for Aerospace Automation (ARCAA). He holds a Bachelor of Engineering (Aerospace Avionics) degree from Queensland University of Technology and Private Pilot’s License (CASA). His research interests include robotic vision and model predictive control for autonomous aircraft (UAS) guidance and navigation.

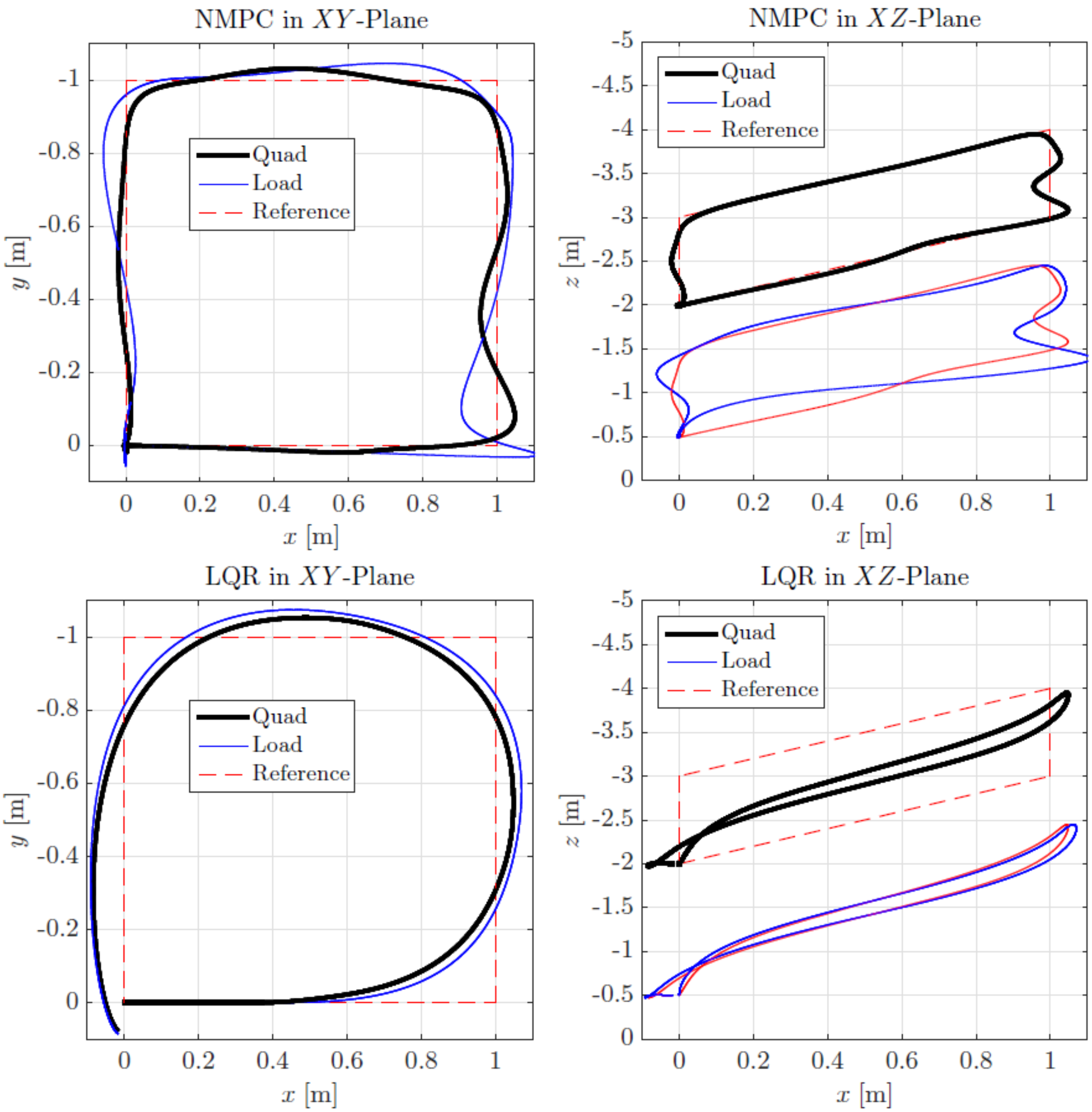

Figure 9. Reference trajectory tracking of LQR and NMPC in comparison the load's reference circular path. The NMPC's performs with an overall RMSD of quad and load position of 0:779m and 0:915m respectively. The LQR comes to 0:781m and 0:924 m.